

**Deuterium atoms and molecules in nanoclusters of molecular deuterium**E. P. Bernard,<sup>1</sup> R. E. Boltnev,<sup>1,2</sup> V. V. Khmelenko,<sup>1</sup> V. Kiryukhin,<sup>3</sup> S. I. Kiselev,<sup>1</sup> and D. M. Lee<sup>1</sup><sup>1</sup>*Laboratory of Atomic and Solid State Physics, Cornell University, Ithaca, New York 14853, USA*<sup>2</sup>*Branch of Institute of Energy Problems of Chemical Physics, Russian Academy of Sciences, Chernogolovka, Moscow Region 142432, Russia*<sup>3</sup>*Department of Physics and Astronomy, Rutgers University, Piscataway, New Jersey 08854, USA*

(Received 24 July 2003; revised manuscript received 6 November 2003; published 15 March 2004)

Impurity-helium solids created by injecting deuterium atoms and molecules into superfluid  $^4\text{He}$  have been studied via x-ray-diffraction and electron-spin-resonance (ESR) techniques. X-ray-diffraction measurements show that these solids are highly porous gel-like structures consisting of  $\text{D}_2$  clusters with the characteristic cluster size of  $90 \pm 30 \text{ \AA}$ . The densities of  $\text{D}_2$  molecules in the samples are  $7 \times 10^{20} - 3 \times 10^{21} \text{ cm}^{-3}$ . Each of the  $\text{D}_2$  clusters are either partially or totally surrounded by thin layers of adsorbed helium which may play an important role in preventing the coalescence of the clusters into larger crystallites of solid  $\text{D}_2$ . Using ESR, we find that *average* concentrations of D atoms of order  $1 \times 10^{18} \text{ cm}^{-3}$  can be achieved in our samples. Measurements of the ground-state spectroscopic parameters and relaxation times of atomic deuterium show that the D atoms reside in the  $\text{D}_2$  clusters. The combined x-ray and ESR data show that *local* concentrations of D atoms as large as  $2 \times 10^{19} \text{ cm}^{-3}$  are obtained in our experiments. The highly porous deuterium nanostructures studied in this work are promising for the production of high concentrations of ultracold neutrons and for significant nuclear polarization of  $\text{D}_2$  molecules by the “brute force method” at low temperatures.

DOI: 10.1103/PhysRevB.69.104201

PACS number(s): 67.40.Yv, 67.40.Mj, 62.65.+k

**I. INTRODUCTION**

By introducing impurity atoms and molecules into a volume of superfluid helium, mesoporous impurity-helium (Im-He) solids can be produced.<sup>1,2</sup> These porous solids are very promising for studying the properties of superfluidity of  $^3\text{He}$  and  $^4\text{He}$  confined in highly disordered environments,<sup>3,4</sup> for matrix isolation of high concentrations of different free radicals,<sup>1,5</sup> and for studies of low temperature chemical tunneling reactions.<sup>6,7</sup> The structure of impurity-helium solids created by the injection of relatively heavy impurities such as neon and krypton atoms and nitrogen molecules has been studied via x-ray-diffraction<sup>8-10</sup> and by means of ultrasound propagation through the liquid  $^4\text{He}$  contained in the pores of the samples.<sup>10-14</sup> It was found that these solids consist of nanoclusters of impurities with typical size  $50-60 \text{ \AA}$  covered by one or two layers of solid helium. The nanoclusters are believed to be assembled into a semirigid porous network of clumps connected by strands. The structure appears similar to light aerogel. The pore size distribution is very broad, from  $80 \text{ \AA}$  to at least  $8600 \text{ \AA}$ , and the average density of impurities in the solids is  $\sim 10^{20} \text{ cm}^{-3}$ .

Up to date, no information has been obtained about the structure of impurity-helium solids formed from light atoms and molecules of hydrogen isotopes, even though these quantum impurity-helium solids are of special interest. Impurity-helium solids with stabilized H and D atoms in mixed  $\text{H}_2/\text{D}_2$  clusters provide an excellent laboratory for studies of low-temperature chemical reactions.<sup>15-17</sup> In particular, the exchange tunneling reactions  $\text{D} + \text{H}_2 \rightarrow \text{HD} + \text{H}$  and  $\text{D} + \text{HD} \rightarrow \text{D}_2 + \text{H}$  have been used to generate high concentrations of hydrogen atoms in impurity-helium solids.<sup>18,19</sup> In deuterium-helium solids, high concentrations of D atoms were achieved directly after formation. The fact that all previous attempts to investigate the structures of impurity-

helium solids formed from light atoms and molecules failed to produce reliable results<sup>10,13,20</sup> motivated the present work.

The creation of macroscopic pure hydrogen-helium solids inside superfluid helium is a very sophisticated problem. Early work concluded that Im-He solids form properly only when the condensed solid is immersed in superfluid helium.<sup>2</sup> Some material containing hydrogen forms and resides on the surface of superfluid  $^4\text{He}$  during hydrogen-helium gas mixture condensation. Hydrogen-helium solids are expected to float on the surface of superfluid  $^4\text{He}$  due to their small density (the density of solid  $\text{H}_2$  is  $0.08 \text{ g/cm}^3$  and the density of superfluid helium at  $T = 1.5 \text{ K}$  is  $0.145 \text{ g/cm}^3$ ). Only when heavier impurities such as Ne atoms or  $\text{D}_2$  molecules are added to hydrogen-helium gas mixtures is it possible to create mixed impurity-helium solids containing atomic and molecular hydrogen with a density larger than the density of He II.<sup>16,17</sup> In contrast to pure hydrogen-helium samples, pure deuterium-helium samples have densities larger than the density of He II and can readily be created inside a volume of superfluid helium.

We have employed x-ray-diffraction and electron-spin-resonance (ESR) techniques to investigate the structure and behavior of impurity-helium solids created by introducing deuterium atoms and molecules into superfluid  $^4\text{He}$ . We have also investigated mixed  $\text{D}_2$ -Ne-He samples to compare the sizes and behavior of clusters created when neon and deuterium were simultaneously present in the gas mixture.

From the x-ray-diffraction experiments, we found that  $\text{D}_2$ -He and  $\text{D}_2$ -Ne-He samples have characteristic impurity densities of order  $\sim 10^{21} \text{ cm}^{-3}$  and that they consist of clusters of impurities with diameters of order  $50-90 \text{ \AA}$ . Using ESR, we have studied the ground-state spectroscopic parameters, line shapes, relaxation times, and saturation behavior of stabilized D atoms in  $\text{D-D}_2$ -He and  $\text{D-D}_2$ -Ne-He solids. Complementary results from x-ray and ESR measurements

allowed us to characterize the properties of Im-He solids created with light impurities. The small clusters of  $D_2$  molecules surrounded by thin layers of solid helium contain the stabilized D atoms. These clusters aggregate into porous gel-like structures similar to the structure of Im-He solids created with heavier atoms and molecules.<sup>10</sup>

Using ESR we also measured the average concentration of D atoms in D- $D_2$ -He samples to be  $\sim 1.5 \times 10^{18} \text{ cm}^{-3}$  and the local concentration (*in the  $D_2$  clusters*) of D atoms to be  $\sim 2 \times 10^{19} \text{ cm}^{-3}$ . High local concentrations of D atoms within  $D_2$  clusters obtained in this work imply that for temperatures  $\leq 175 \text{ mK}$  this system is close to the regime where the mean distance ( $d_m \sim 38 \text{ \AA}$ ) between D atoms is comparable to the thermal de Broglie wavelength for free D atoms.

It is found, however, that the recombination rate of deuterium atoms in D- $D_2$ -He impurity-helium solids is quite slow,<sup>16</sup> indicating a very small rate of diffusion and hence a high degree of localization of D atoms in Im-He solids. This does not augur well for the possible observation of quantum overlap in these solids unless much higher concentrations of D atoms can be achieved. Nevertheless studies of D atoms in Im-He solids are useful in providing a model system for Im-He solids containing H atoms. We believe that Im-He solids containing H atoms and molecules provide much more promising systems for investigating quantum overlap effects because of a higher degree of delocalization of H atoms due to the highly efficient  $H + H_2 \rightarrow H_2 + H$  tunneling exchange reaction.<sup>16,21</sup>

At the present time no one has been able to create Im-He solids inside He II containing exclusively  $H_2$  and H impurities. In our laboratory we are developing methods to produce such a sample. Our approach will involve the use of magnetic gradients to draw samples containing the paramagnetic hydrogen atoms into the superfluid helium. Preliminary experiments involving manipulation of impurity-helium solids via field gradients have recently been performed in our laboratory.<sup>22</sup>

The unique properties of Im-He solids containing light atoms and molecules may lead to specialized applications. A proposal made by Nesvizhevsky<sup>23</sup> is to use  $D_2$ -He and  $D_2O$ -He solids as media for obtaining ultracold neutrons. Very cold (1 mK)  $D_2$ -He solids should be able to act as extremely efficient moderators, allowing a two order of magnitude improvement in the available flux of ultracold neutrons. The solids obtained in our experiments satisfy three essential criteria for such a moderator: nanoscale building blocks (the clusters), high porosity, and low absorption of neutrons.

Frossati and co-workers<sup>24–26</sup> suggested another application in which the D- $D_2$ -He solids are cooled to low enough temperatures ( $\sim 3 \text{ mK}$ ) in very high magnetic fields to produce “brute-force” nuclear polarization. Spin polarized deuterium nuclei are expected to be able to enhance the efficiency of fusion reactions involving deuterons.

## II. EXPERIMENTAL METHOD

We created the impurity-helium solids using a technique described in more detail elsewhere.<sup>2,10</sup> In this technique, a jet

of helium gas containing a small fraction (1–5%) of impurity atoms and/or molecules was directed onto the surface of superfluid  $^4\text{He}$  contained in a small beaker sitting above a main helium bath at  $T \sim 1.5 \text{ K}$ . The distance between the orifice of the gas jet source and the surface of He II was  $\sim 2 \text{ cm}$ . The jet penetrated the surface of the liquid helium and a macroscopic snowlike semitransparent material was created. This material fell down through the liquid  $^4\text{He}$  to form a porous solid at the bottom of the beaker. A jet with a flux of  $\sim 5 \times 10^{19}$  atoms and molecules per second yielded  $\sim 0.3\text{--}0.4 \text{ cm}^3$  of sample in 10 min.

The conditions described above were found to be optimal for the preparation of impurity-helium solids. To find these conditions, we studied the efficiency of Im-He sample collection in superfluid  $^4\text{He}$  as a function of four independent parameters. Collection temperatures of the liquid helium were varied from  $T = 1.2$  to  $1.8 \text{ K}$ ; accordingly the helium vapor pressure in the Dewar was varied from 0.625 to 12.5 Torr. The flux of the condensed gas mixture was varied from  $10^{18}$  to  $10^{20}$  atoms(molecules)/s. The concentration of impurities in the gas make-up mixtures was varied from 0.1 to 5%, a small fraction in comparison with the amount of helium gas. The distance between the source orifice and the He surface in the beaker was varied from 1.5 to 3 cm. The efficiency of sample collection was determined by monitoring the collection process visually in a glass Dewar. In particular, it was found that increasing the temperature above 1.5 K led to decreased efficiency because the higher vapor pressure causes an increase in scattering of the gas jet. This scattering can lead to the impurity atoms or molecules becoming entrained in the counterflow of the evaporating liquid helium. Decreasing the temperature below 1.5 K led to the production of unstable samples which tended to explode spontaneously even when surrounded by superfluid helium. More careful quantitative investigations of the sample preparation process will be undertaken with a closed cell geometry<sup>26</sup> presently being developed in our laboratory.

Impurity-helium samples for x-ray investigation were collected in a beryllium beaker<sup>8,10</sup> inside a pumped helium cryostat designed for x-ray-diffraction measurements. The cryostat was mounted on a two-circle goniometer and the experiment was performed in a standard horizontal scattering geometry. X-ray scattering measurements were carried out on beamline X22B at the National Synchrotron Light Source at Brookhaven National Laboratory. The energy of the x-rays was 7.861 keV. The diffraction patterns produced by the impurity-helium samples are essentially powder diffraction patterns, so standard  $\theta$ - $2\theta$  scans were used for data collection. After impurity-helium sample collection was finished, the sample was maintained in liquid helium at  $T = 1.5\text{--}4.2 \text{ K}$ , or alternatively liquid helium was drained from the cell. The latter procedure forms what is known as a “dry” sample, in which the porous solid no longer contains liquid helium.

For subsequent data analysis, standard corrections for polarization and sample volume were made. To isolate the scattering due to the Im-He solid sample from the scattering due to liquid helium, the sample cell, and the cryostat windows, each experiment consisted of two sets of measurements. First

the sample was prepared and x-ray measurements were carried out. Then the sample was evaporated by heating the sample cell to a high temperature, and the measurements were repeated at low temperature both for the cell filled with liquid helium and for the empty cell. The former “background” scans were used for the samples immersed in liquid helium, while the latter were used for the dry sample. These background x-ray scans were subtracted from the Im-He sample data.

Impurity-helium solids with stabilized D atoms for ESR investigations were prepared *in situ* in a Janis cryostat. Samples were produced by sending a gaseous mixture of helium with typically a (1%) admixture of molecular deuterium through a high-frequency electric discharge ( $f = 52$  MHz,  $P = 70$  W) into superfluid helium contained in a small quartz beaker as described in detail previously.<sup>15</sup> At the end of the collection process the Im-He sample occupied all of the cylindrical part of the beaker. After sample preparation, the beaker containing the sample was lowered into the ESR cavity, which was situated at the bottom of the cryostat in the homogeneous field region of a Varian 7800 electromagnet. The volume occupied by the sample inside the cavity was  $0.35$  cm<sup>3</sup>. The homemade cylindrical cavity was operated in the TE<sub>011</sub> mode. ESR signals were recorded by using a continuous wave reflection homodyne spectrometer (Varian E-4) operating near 9.1 GHz. The microwave carrier frequency was measured by using a frequency counter (EIP 545) while the field was swept through each resonance. Derivatives of the ESR absorption lines were detected at  $\sim 0.32$  T by the addition of a small amplitude modulation field oscillating at 100 kHz.

Atomic concentrations were measured by comparing the intensity of the atomic signals with the intensity of a signal from a small ruby crystal that was used as a secondary standard. The ruby crystal was attached permanently to the bottom of the microwave cavity. The calibration of the absolute value of the number of spins in ruby crystal was made by using a standard organic diphenyl-picrylhydrazil (DPPH) sample with a known number ( $2.4 \times 10^{17}$ ) of spins. The calibration measurements were carried out at  $T = 1.35$  K and  $T = 1.8$  K.

A nuclear magnetic resonance (NMR) magnetometer (“Sentec” type 1001) was used for precise measurements of magnetic field. The distribution of magnetic field in the electromagnet was mapped by removing the cryostat from the magnet gap and moving the NMR probe throughout the gap. The relative homogeneity of the magnetic field at the value 0.32 T over the volume of the sample was  $3.1 \times 10^{-6}$ . From the measured ESR signal of DPPH with known  $g$  factor ( $g = 2.0037$ ) at the temperature 1.35 K, the difference of the magnetic field between the position of the sample (in the center of magnet) and the position of the NMR probe located outside cryostat was determined to be 1.58 G. This value has been taken into account in the analysis of all ESR spectra of D atoms recorded at low temperatures.

By reducing the supply of liquid helium into the variable temperature insert (VTI) of our cryostat we lowered the level of liquid helium. When the level was below the ESR cavity we investigated dry impurity-helium samples at different

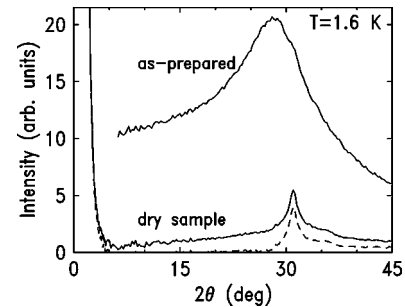


FIG. 1. X-ray-diffraction patterns for the as-prepared D<sub>2</sub>-He sample immersed in liquid helium (top curve), and the dry sample (bottom solid curve) at  $T = 1.6$  K. The dashed line shows the data for the dry sample after the signal due to the liquid helium captured in the sample was subtracted, as discussed in the text.

temperatures. A LakeShore 330 temperature controller was used to control and stabilize the temperature of the sample.

### III. EXPERIMENTAL RESULTS

#### A. X-ray measurements

We performed x-ray investigations on three D<sub>2</sub>-He samples immediately after preparation (one formed by using the gas mixture [D<sub>2</sub>]:[He]=1:20 and two by using the gas mixture [D<sub>2</sub>]:[He]=1:40), and one D<sub>2</sub>-Ne-He sample (formed using the mixture [D<sub>2</sub>]:[Ne]:[He]=1:4:500). The diffraction patterns of D<sub>2</sub>-He samples immediately following formation were very weak (see Fig. 1). One of the D<sub>2</sub>-He samples (prepared with the gas mixture [D<sub>2</sub>]:[He]=1:40) was drained of superfluid He and gradually warmed from 1.6 K to 8 K. In this sample the dynamics of the growth of clusters of D<sub>2</sub> molecules in D<sub>2</sub>-He solids was studied. In the case of the D<sub>2</sub>-Ne-He sample, the diffraction pattern was observed only at  $T = 1.6$  K, because this sample spontaneously decomposed during the process of warming to 4 K while immersed in liquid <sup>4</sup>He.

We begin by discussing the D<sub>2</sub>-He samples. Figure 1 shows the diffraction data collected immediately after sample preparation (the “as-prepared” sample) and the data for the dry sample. Both measurements were made at  $T = 1.6$  K. The diffraction data for the as-prepared sample is dominated by a strong and very broad peak centered at  $2\theta \approx 28^\circ$ . This peak is due to scattering from the liquid helium filling the bulk of the sample cell. A very weak shoulder at  $2\theta \approx 31^\circ$  is also observed. As liquid helium is removed from the sample cell, this feature grows and becomes a well-defined peak in the dry sample. The peak at  $2\theta \approx 31^\circ$  is at the position of the (111) Bragg peak of the fcc phase of solid D<sub>2</sub> and therefore arises due to the presence of solid deuterium in the sample. The D<sub>2</sub> signal in the as-prepared sample is too weak to be quantitatively analyzed. Below, we present the analysis of the dry sample data.

First, we note that our highly porous samples possess a very large internal surface because of the nanometer scale of the typical impurity block of which these samples are built. Therefore it is expected that a significant amount of helium is trapped on the D<sub>2</sub> surface and in the sample pores even

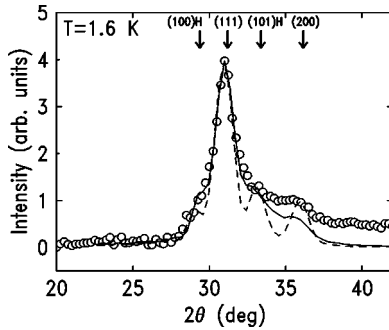


FIG. 2. X-ray-diffraction pattern indicated by open circles for the dry  $D_2$ -He sample, where the signal due to the liquid helium captured in the sample has been subtracted. The temperature is 1.6 K. The solid line is the result of the calculation for 90 Å clusters with stacking faults, as described in the text. The dashed line is the result of the calculation for a 2:1 mixture of 75 Å fcc and hcp clusters with no defects. The positions of the Bragg peaks in the fcc and hcp bulk solid  $D_2$  are shown at the top of the figure.

when liquid helium is drained from the sample cell. Indeed, a broad background closely resembling the scattering signal of liquid helium is clearly present underneath the deuterium peak in the dry-sample data of Fig. 1. When an appropriately scaled liquid helium background is subtracted from the dry sample data, no signal is left in a broad range of scattering angles. The best results, shown with the dashed curve in Fig. 1, were obtained assuming that approximately 8% of the helium initially present in the cell remains in the dry sample. After the helium signal subtraction, virtually no scattering intensity is left for  $5^\circ < 2\theta < 25^\circ$ . This result strongly suggests that this broad background can indeed be attributed to helium scattering.

The x-ray signal remaining after the background subtraction described above can be attributed to scattering from deuterium. This intensity is shown on an expanded scale in Fig. 2. Solid  $D_2$  crystallizes in the fcc, hcp, and mixed close-packed structures, depending on the volume fraction of para- $D_2$  and on the cooling rate during sample preparation procedure.<sup>27</sup> Features characteristic of these structures are clearly seen in the data of Fig. 2, most notably the broad peaks at the (111) and (200) Bragg peak positions of the fcc solid  $D_2$  ( $2\theta \approx 31^\circ$  and  $2\theta \approx 36^\circ$ , respectively). A weaker but still identifiable signal is also present at the (100) and (101) hcp Bragg peak positions ( $2\theta \approx 29.5^\circ$  and  $33.5^\circ$ ). Similar diffraction patterns were previously observed in impurity-helium samples composed of heavy impurities crystallized in close-packed structures, such as Ne,  $N_2$ , and Kr.<sup>8,10</sup> Analysis of the x-ray data in these samples has shown that they consist of nanometer-scale clusters of the impurity atoms assembled into a rigid porous network.<sup>8,10</sup> The close-packed structures of these clusters were found to possess a large number of stacking-fault defects.

In the presence of defects, there is no simple quantitative relationship between the width of the diffraction profiles and the cluster size. To determine the typical  $D_2$  cluster size and the density of our samples, we follow the analysis of Refs. 8, 10. We consider close-packed clusters (fcc or hcp) containing a specified number of stacking faults. The intensity

for the scattering vector  $k$  from a collection of such clusters randomly oriented in space is given by the Debye scattering equation<sup>28</sup>

$$I = I_0 P V e^{-2M} \sum_m \sum_n f^2(k) \frac{\sin(kr_{mn})}{kr_{mn}}. \quad (1)$$

Here  $P = \cos^2(2\theta)$  is the polarization factor,  $V = 1/\sin(2\theta)$  is the sample volume correction,  $r_{mn}$  is the distance between the  $m$ th and  $n$ th atoms, and  $f(k)$  is the atomic factor of deuterium. The factor  $e^{-2M}$  arises due to lattice dynamics effects and is discussed later. The calculated diffraction patterns were averaged over the possible positions of the stacking faults in the cluster.

To simplify the calculations, rotational degrees of freedom of the  $D_2$  molecules in the clusters were disregarded. Thus, we considered model structures that had two deuterium atoms located at each point of the close-packed lattice of the cluster. This approximation is chiefly justified by the almost spherical molecular charge distribution of deuterium.<sup>29</sup> We also note that this simplified model was previously found to adequately describe the experimental results for  $N_2$ -He samples in the range of scattering vectors accessible in our work.<sup>10</sup>

We used the standard harmonic approximation to take into account the lattice dynamics effects. In this approximation, the diffracted intensity is reduced by a factor  $e^{-2M}$ , where  $2M = 12h^2T \sin^2(\theta) [\Phi(x) + x/4] / (mk\theta_m^2\lambda^2)$ .<sup>28</sup> Here  $x = \theta_m/T$ ,  $\Phi(x) = 1/x \int_0^x \epsilon(e^\epsilon - 1)^{-1} d\epsilon$ ,  $m$  is the mass of the  $D_2$  molecule, and  $\theta_m \approx 109$  K is the Debye temperature of deuterium.<sup>29</sup> This approximation almost certainly underestimates the thermal vibrations in our samples because a substantial fraction of molecules reside at the cluster surfaces. Quantum effects should also reduce the observed intensity. We note, however, that introduction of the  $e^{-2M}$  factor does not affect the cluster size obtained in our calculations, and changes the calculated density of  $D_2$  by a factor less than 1.5. We therefore conclude that errors due to the inadequate treatment of the lattice dynamics do not affect our analysis significantly.

The best agreement with the experimental data shown in Fig. 2 was obtained for clusters consisting of  $\sim 11\,500$   $D_2$  molecules (diameter  $\sim 90$  Å). The solid line in Fig. 2 shows the calculation made for 90 Å clusters, modeling 60% of the clusters with a randomly stacked structure and 40% of the clusters with an fcc structure containing three twin faults. The number of defects in the clusters given above should, of course, be taken only as an estimate. We note that the defects are necessary to explain the experimental data, because calculations for defect-free clusters reproducing the width of the (111) fcc peak always produce much narrower (200) fcc and (101) hcp peaks than those found experimentally. To illustrate this point, the calculation for a 2:1 mixture of 75 Å fcc and hcp clusters with no defects is shown in Fig. 2 as a dashed line. Clearly, it is in worse qualitative agreement with the experimental results than the calculation for clusters with defects. We note that all the calculations using the close-packed models underestimate the diffraction signal for  $2\theta > 34^\circ$ . Some possible reasons for this discrepancy are the

disregard of the rotational degrees of freedom of the  $D_2$  molecules, the restriction of the trial structures to the close-packed type, and errors in the model used for the background subtraction procedure.

The lower limit on the cluster size can be estimated from the calculations for defect-free clusters discussed above because disordered clusters always produce broader peaks than the ideal clusters of the same size. The upper limit on the cluster size can be estimated from the calculation for clusters with random close-packed structure (the most disordered clusters). Such calculations averaged over a number of random distributions of the defects produce a (111) fcc peak which is narrower than the one observed experimentally for clusters 130 Å in diameter and larger. Thus, we conclude that the typical size of the  $D_2$  building block in our samples is between 75 Å and 130 Å, with the most likely size of 90 Å. It is also possible that a small fraction of the clusters contained in the samples are of smaller sizes. From the comparison of the intensity calculated using our best model (the solid line in Fig. 2) with the scattering from liquid helium, we estimate that the average deuterium density in the sample is  $\sim 2.5 \times 10^{21}$  molecules/cm<sup>3</sup>. This is approximately 12 times smaller than the density of bulk solid  $D_2$ .

The density of as-prepared samples must be much smaller than that of the dry samples since the intensity of the  $D_2$  signal is very small in the former (see Fig. 1). Assuming that the as-prepared samples contain  $D_2$  clusters of the same size as those in the dry samples, one can estimate (from Fig. 1) that the integrated  $D_2$  signal is roughly an order of magnitude smaller in the as-prepared samples. Thus, a rough estimate of the deuterium density in these samples is  $\sim 10^{20}$  cm<sup>-3</sup>. However, we note that our measurements lack the sensitivity necessary to detect smaller  $D_2$  clusters in the as-prepared samples, and therefore the actual  $D_2$  density in these samples can be significantly larger.

Similar to the previously investigated Ne-He and  $N_2$ -He samples,<sup>8,10</sup> the  $D_2$ -He samples exhibit the nanoscale size of a typical impurity-species building block and low volume density. Thus, these samples must be highly porous and possess a large internal surface. In fact, if we assume that the dry  $D_2$  sample discussed above consists of a collection of disconnected 90 Å clusters, its internal deuterium surface should be  $\sim 50$  m<sup>2</sup> per cm<sup>3</sup>. The interaction energy of helium with the solid  $D_2$  substrate is of the order of 20 K,<sup>30</sup> and therefore an atomic layer of helium is expected to be trapped on the surface of our sample. Such an adsorbed monolayer of helium can account for approximately a quarter of all the helium trapped in the sample. The remaining helium must be contained in the sample pores. While the above calculation probably overestimates the sample internal surface, it is clear that a significant fraction of the trapped helium is adsorbed on the sample surface. The adsorbed helium should survive at elevated temperatures, especially in the samples made of heavy impurities ( $N_2$ , Kr, etc.).

The dry  $D_2$  samples are stable at  $T=1.6$  K. The samples, however, quickly coalesce and form a powder with a macroscopic grain size at higher temperatures. Figure 3 shows the data for  $T=3.2$  K. The background due to liquid helium trapped in this sample (3.5% of the bulk helium density) is

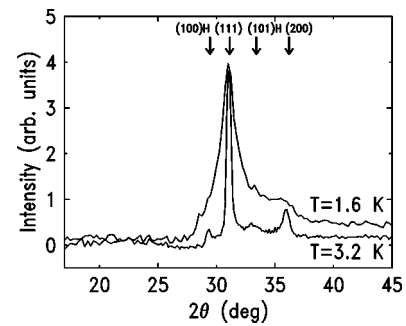


FIG. 3. X-ray-diffraction patterns for the dry  $D_2$ -He sample at  $T=1.6$  K and  $T=3.2$  K. The signal due to the liquid helium captured in the sample is subtracted as discussed in the text.

subtracted from these data. A mixture of the fcc and hcp structures is observed, consistent with earlier studies of bulk deuterium.<sup>27</sup>

Finally, we briefly discuss experiments with a mixed  $D_2$ -Ne-He sample. The sample was prepared using a 1:4:500 Ne- $D_2$ -He gas mixture. The x-ray-diffraction pattern for this sample immersed in liquid helium is shown in Fig. 4(a). The liquid helium background is subtracted. The diffraction pattern consists of two overlapping peaks indicating that both neon and deuterium clusters are present in the sample. Because the peaks overlap, it is impossible to determine whether mixed clusters exist in the sample. We find that the neon signal (the peak at larger scattering angles) can be described very satisfactorily using a model structure consisting of  $\sim 50$  Å fcc clusters, each with four deformation-type stacking faults. The result of this model calculation is shown as a solid line in Fig. 4(a). To obtain the deuterium signal, we

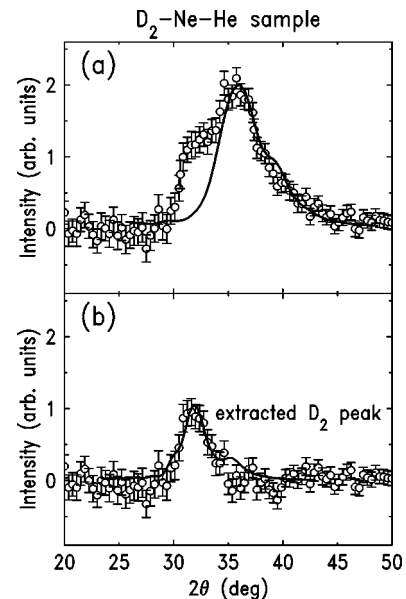


FIG. 4. (a) X-ray-diffraction pattern for the  $D_2$ -Ne-He sample at  $T=1.6$  K. Liquid helium background is subtracted. The solid line is the result of the calculation for 50 Å neon clusters with faults, as described in the text. (b) The same data with the calculated neon signal subtracted. The solid line is the result of the calculation for 75 Å compressed  $D_2$  clusters with faults, as described in the text.

TABLE I. Initial concentrations  $n_a$ , ESR linewidths  $\Delta H_{pp}$ , and magnetic parameters for D atoms in Im-He solids obtained from this work. All spectra were recorded at a microwave power of  $P_c = 2.25 \mu\text{W}$ . Additional results for samples marked with superscript numbers are presented in Figs. 5–10.

Gas mixture	Sample	$n_a$ , per $\text{cm}^3$	$\Delta H_{pp}$ , Gauss	$g$ -factor	$\Delta W$ , MHz	$A$ , MHz
$[\text{D}_2]:[\text{He}] = 1:20$	D-D <sub>2</sub> -He <sup>(1)</sup>	$1.5 \times 10^{18}$	1.8–1.9	2.002202(16)	326.431(56)	217.621(38)
$[\text{D}_2]:[\text{He}] = 1:20$	D-D <sub>2</sub> -He	$1.2 \times 10^{18}$	1.8–1.9			
$[\text{D}_2]:[\text{He}] = 1:20$	D-D <sub>2</sub> -He	$1.2 \times 10^{18}$	1.8–1.9			
$[\text{D}_2]:[\text{He}] = 1:100$	D-D <sub>2</sub> -He <sup>(2)</sup>	$6.5 \times 10^{17}$	1.7–1.8	2.002197(17)	326.482(63)	217.655(42)
$[\text{D}_2]:[\text{He}] = 1:100$	D-D <sub>2</sub> -He	$4.0 \times 10^{17}$	1.7–1.8	2.002219(26)	326.505(40)	217.670(26)
$[\text{D}_2]:[\text{He}] = 1:100$	D-D <sub>2</sub> -He <sup>(3)</sup>	$4.5 \times 10^{17}$	1.7–1.8	2.002170(34)	326.494(97)	217.663(65)
$[\text{Ne}]:[\text{D}_2]:[\text{He}] = 1:4:500$	D-D <sub>2</sub> -Ne-He <sup>(4)</sup>	$1.5 \times 10^{17}$	2.1	2.002227(37)	326.406(98)	217.604(65)
$[\text{Ne}]:[\text{D}_2]:[\text{He}] = 1:4:500$	D-D <sub>2</sub> -Ne-He	$2 \times 10^{17}$	2.2–2.4	2.002204(28)	326.494(53)	217.663(35)
$[\text{Ne}]:[\text{D}_2]:[\text{He}] = 1:4:500$	D-D <sub>2</sub> -Ne-He	$1.5 \times 10^{17}$	1.9			

subtract the calculated neon signal from the data. The result obtained is shown in Fig. 4(b). These data can be described using a model structure with  $\sim 75 \text{ \AA}$  fcc D<sub>2</sub> clusters with five deformation-type faults [as indicated by the solid line in Fig. 4(b)]. However, to fit the data the calculated deuterium peak must be shifted to larger scattering angles by  $\sim 0.8^\circ$ . While this shift can simply result from an inadequate modeling of the neon signal, it may also indicate that the cluster average lattice constant is smaller by  $\sim 1\text{--}2\%$  than that of solid D<sub>2</sub> (the clusters are compressed). Thus it is possible that a small admixture of neon is present in the D<sub>2</sub> clusters. Using the ratio of the neon and deuterium signals to the scattering signal of liquid helium, and utilizing the structural models described above, we find the neon atom and deuterium molecule densities to be  $3 \times 10^{19} \text{ atoms/cm}^3$  and  $7 \times 10^{20} \text{ molecules/cm}^3$ , respectively.

In summary, x-ray scattering studies described above show that the D<sub>2</sub>-He and D<sub>2</sub>-Ne-He samples prepared in our work are highly porous solids with nanometer-scale typical building blocks. The samples exhibit strongly disordered structures. The typical deuterium cluster size is estimated to be  $\sim 90 \text{ \AA}$  in the dry deuterium sample investigated and  $\sim 75 \text{ \AA}$  in the D<sub>2</sub>-Ne-He sample immersed in liquid helium. In these samples, the deuterium densities are  $\sim 2.5 \times 10^{21}$  and  $\sim 7 \times 10^{20} \text{ molecules/cm}^3$ , respectively. A significant amount of helium is trapped in the dry samples at low temperatures. We argue that a large fraction of this helium is adsorbed on the internal sample surface.

### B. ESR measurements

We also performed ESR investigations of the samples formed by injecting into He II three different gas mixtures— $[\text{D}_2]:[\text{He}] = 1:20$ ,  $[\text{D}_2]:[\text{He}] = 1:100$ , and  $[\text{Ne}]:[\text{D}_2]:[\text{He}] = 1:4:500$ . Three samples formed from each gas mixture were studied. The rf discharge was adjusted to maximize the concentration of stabilized atoms in each resulting sample. The initial concentrations  $n_a$ , ESR linewidths  $\Delta H_{pp}$ , gyromagnetic ratios  $g$ , zero-field hyperfine splittings  $\Delta W$ , and hyperfine constants  $A$  of deuterium atoms in Im-He solids investigated in this work are presented in Table I. The reproducibility of the initial concentrations of D atoms

formed by each particular gas mixture was better than 30%, and the reproducibility of the ESR linewidth was  $\sim 20\%$ .

#### 1. Measurements of $g$ factor and $A$ values of D atoms in Im-He solids

Figure 5(a) shows a plot of the energy levels of deuterium atoms versus magnetic field. The dependence of the D atom energy levels on magnetic field was calculated following the Breit-Rabi formula.<sup>31</sup> For D atoms this formula can be written in the following form:

$$E(F, M) = \frac{\Delta W}{6} + g_I \mu_0 H M \pm \frac{\Delta W}{2} \sqrt{1 + \frac{4Mx}{3} + x^2}, \quad (2)$$

where  $E(F, M)$  is the energy of the D atom state with the total angular momentum  $F$  and its projection  $M$  along the magnetic field,  $\Delta W$  is the zero-field hyperfine splitting between the two multiplets,  $F = \frac{3}{2}$  and  $F = \frac{1}{2}$ , and  $x$  is given by

$$x = \frac{g_J - g_I}{\Delta W} \mu_0 H. \quad (3)$$

In the above expression,  $\mu_0$  is the Bohr magneton, and the spectroscopic splitting factors  $g_J$  and  $g_I$  are related to the electron and nuclear magnetic moments  $\vec{\mu}_J$  and  $\vec{\mu}_I$  by

$$\vec{\mu}_J = -g_J \mu_0 \vec{J}, \quad \vec{\mu}_I = -g_I \mu_0 \vec{I}. \quad (4)$$

The plus sign in Eq. (2) is used when  $F = \frac{3}{2}$ , and the minus sign when  $F = \frac{1}{2}$ . The allowed transitions with  $\Delta M = \pm 1$  and  $\Delta I_z = 0$  (where  $I_z$  is the projection of nuclear spin along the magnetic field  $\vec{H}$ ) give the three hyperfine structure lines of the D atom ESR spectrum [Fig. 5(a)] in the  $(F, M)$  representation:

$$(F = \frac{3}{2}, M = \frac{3}{2} \leftrightarrow F = \frac{1}{2}, M = \frac{1}{2}), \quad I_z = 1,$$

$$(F = \frac{3}{2}, M = \frac{1}{2} \leftrightarrow F = \frac{1}{2}, M = -\frac{1}{2}), \quad I_z = 0,$$

$$(F = \frac{3}{2}, M = -\frac{1}{2} \leftrightarrow F = \frac{3}{2}, M = -\frac{3}{2}), \quad I_z = -1.$$

Energy values corresponding to these transitions are given by

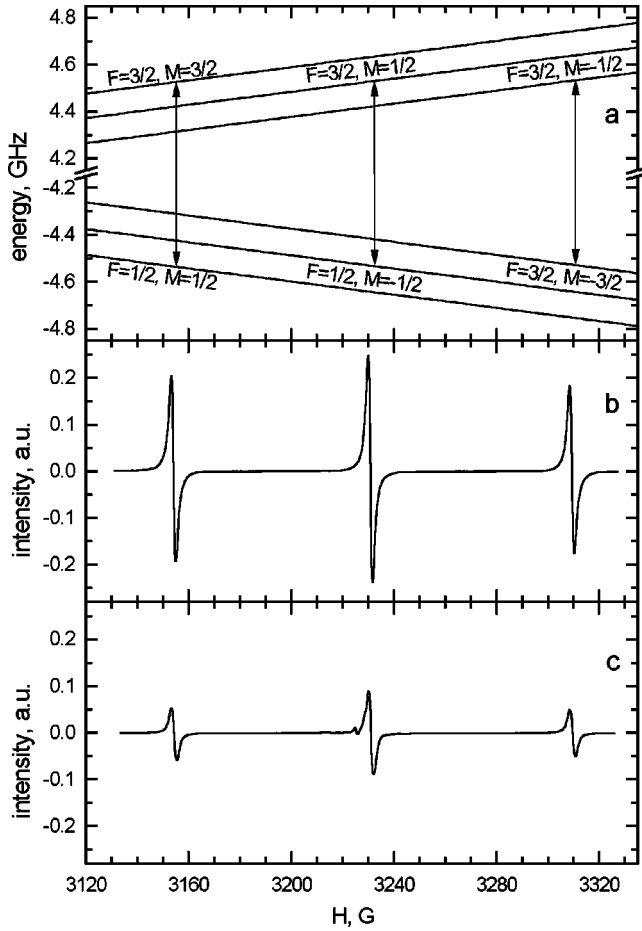


FIG. 5. Magnetic energy levels and allowed ( $\Delta M = \pm 1$ ,  $\Delta I_z = 0$ ) transitions of D atoms in high external magnetic fields (a), ESR spectra of D atoms in as-prepared D-D<sub>2</sub>-He (sample No. 2, see Table I) (b), and D-D<sub>2</sub>-Ne-He (sample No. 4, see Table I) (c); solids created by the gaseous mixtures [D<sub>2</sub>]:[He]=1:100 and [D<sub>2</sub>]:[Ne]:[He]=4:1:500, respectively. These spectra were obtained at  $T = 1.375$  K and klystron frequency  $f_k = 9.064$  GHz.

$$h\nu_1 = \frac{\Delta W}{2} \left( 1 + x_1 + \sqrt{1 + \frac{2}{3}x_1 + x_1^2} \right) - \mu_I H_1, \quad (5)$$

$$h\nu_0 = \frac{\Delta W}{2} \left( \sqrt{1 + \frac{2}{3}x_0 + x_0^2} + \sqrt{1 - \frac{2}{3}x_0 + x_0^2} \right) - \mu_I H_0, \quad (6)$$

$$h\nu_{-1} = \frac{\Delta W}{2} \left( -1 + x_{-1} + \sqrt{1 - \frac{2}{3}x_{-1} + x_{-1}^2} \right) - \mu_I H_{-1}, \quad (7)$$

where  $x_1$ ,  $x_0$ , and  $x_{-1}$  correspond to the nuclear spin states  $I_z = 1, 0, -1$ , respectively. The values of frequencies  $\nu_{-1}$ ,  $\nu_0$ ,  $\nu_1$  and magnetic fields  $H_{-1}$ ,  $H_0$ ,  $H_1$  were measured for the center of each resonance line for D atoms in Im-He solids. To obtain  $g_J$  and  $\Delta W$  a procedure similar to the one described in Ref. 32 was used. All the fundamental physical constants as well as the  $g_I$  value for these calculations were taken from Ref. 33.

The abbreviations  $e_+ = h\nu_1 + \mu_I H_1$ ,  $e_- = h\nu_{-1} + \mu_I H_{-1}$ , and the definition  $r = x_1/x_{-1} = H_1/H_{-1}$  were used for the inversion of Eqs. (5) and (7) into equations

$$\frac{1}{3}x_1\Delta W^2 - (1+x_1)e_+\Delta W + e_+^2 = 0, \quad (8)$$

$$-\frac{1}{3}x_{-1}\Delta W^2 + (r-x_{-1})e_-\Delta W + re_-^2 = 0. \quad (9)$$

Summing these equations leads to

$$\Delta W = \frac{e_+^2 + re_-^2}{x_1(e_+ + e_-) + e_- - re_-}. \quad (10)$$

A quadratic equation in  $x_1$  is formed by substitution of Eq. (10) into Eq. (8),

$$ax_1^2 + bx_1 + c = 0, \quad (11)$$

with

$$a = e_+e_-(e_+ + e_-)(e_+ - re_-),$$

$$b = \frac{1}{3}(e_+^2 + re_-^2)^2 + e_+e_-[(e_+ - re_-)^2 - r(e_+ + e_-)^2],$$

$$c = re_+e_-(e_+ + e_-)(e_+ - re_-).$$

Then  $x_1$  can be easily found from Eq. (11) and substituted into Eq. (10) to determine  $\Delta W$ . The  $g$ -factor values can be obtained from Eq. (3). The  $g$ -factor values,  $\Delta W$  values and hyperfine constants  $A$  (Ref. 34) for deuterium atoms in different impurity-helium solids obtained by the above procedure are listed in Table I. Table II presents data for free D atoms and D atoms stabilized in different matrices at low temperatures taken from Refs. 32, 35–37. The  $g$ -factor values of D atoms stabilized in D-D<sub>2</sub>-He and in D-D<sub>2</sub>-Ne-He solids are close to each other (see Table I) and very similar to the  $g$ -factor values obtained for D atoms in solid D<sub>2</sub> matrices and in the gas phase (see Table II). This leads to the conclusion that most stabilized D atoms in the Im-He samples investigated are not immediately adjacent to Ne atoms but are surrounded by solid D<sub>2</sub> or condensed helium. The following saturation test of ESR signals of D atoms distinguishes these cases.

TABLE II. Magnetic parameters for free D atoms and D atoms in D<sub>2</sub> and Ne matrices.

Sample	$g$ -factor	$\Delta W$ , MHz	$A$ , MHz	Citation
D in gas phase	2.002256(24)	327.384302(30)	218.256201(20)	35
D in D <sub>2</sub> matrix	2.00231(8)	326.57(27)	217.71(18)	36
D in D <sub>2</sub> matrix	2.00220(16)	328.29	218.86(15)	32
D in Ne matrix	2.0020(1)	unavailable	219.0(1)	37

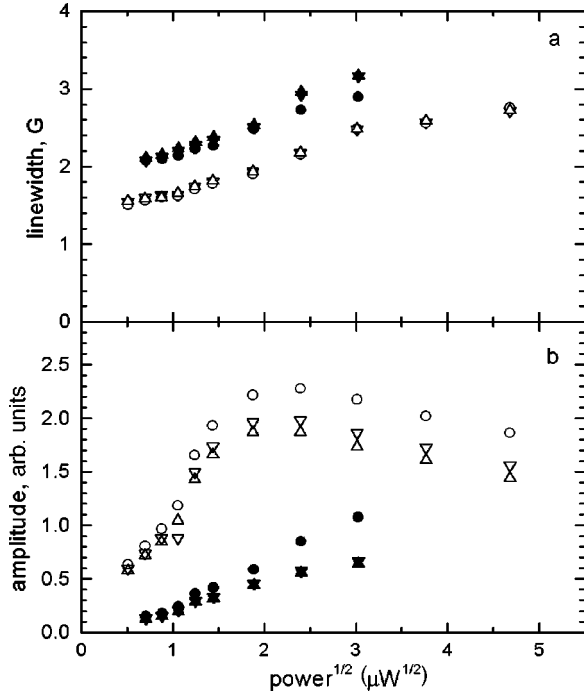


FIG. 6. Linewidth  $\Delta H_{pp}$  (a) and amplitude  $A_{pp}$  (b) of the first derivative of the hyperfine ESR components of D atoms in D-D<sub>2</sub>-He sample (No. 2, see Table I) ( $\nabla$ :  $I_z = +1$ ,  $\circ$ :  $I_z = 0$ ,  $\triangle$ :  $I_z = -1$ ) and in D-D<sub>2</sub>-Ne-He sample (No. 4, see Table I) (closed  $\nabla$ :  $I_z = +1$ , closed  $\circ$ :  $I_z = 0$ , closed  $\triangle$ :  $I_z = -1$ ) as functions of the square root of microwave power.

## 2. Saturation of ESR signals of D atoms

We usually observed the three-component spectra of D atoms in Im-He solids in which the central line amplitude exceeded those of the low-field and high-field lines.<sup>15,17</sup> Figures 5(b) and 5(c) show the ESR spectra of D atoms in as-prepared D-D<sub>2</sub>-He and D-D<sub>2</sub>-Ne-He samples that were taken at a temperature of  $T = 1.37$  K with microwave power  $P_c \sim 2.25 \mu\text{W}$ . In these experiments the D-D<sub>2</sub>-He sample was created by introducing the gas mixture  $[\text{D}_2]:[\text{He}] = 1:100$  with beam flux  $5 \times 10^{19} \text{ s}^{-1}$  from the discharge region into superfluid helium and the D-D<sub>2</sub>-Ne-He sample was created in the same manner by introduction of the gas mixture  $[\text{D}_2]:[\text{Ne}]:[\text{He}] = 4:1:500$  with flux  $6 \times 10^{19} \text{ s}^{-1}$ . A similar ratio between central line and side line amplitudes was observed in D atoms stabilized in solid deuterium at  $T \sim 1.35$  K.<sup>32,36,38</sup> This effect was explained by more efficient saturation of the side lines relative to the central line because of differences in the effective relaxation rates for the transitions between the corresponding sublevel pairs. This difference arises when the relaxation rates for the electron and nuclear spins in the deuterium atoms are comparable.<sup>38</sup> In the case of our samples the increase in the effective relaxation rate for sublevel pairs via additional channels should be greater for the transition ( $F = \frac{3}{2}$ ,  $M = \frac{1}{2} \leftrightarrow F = \frac{1}{2}$ ,  $M = -\frac{1}{2}$ ),  $I_z = 0$ , corresponding to the central line. We carried out investigations of the saturation of the D atom ESR signal in different Im-He solids. Figure 6 shows the dependence of the amplitudes and line widths as obtained from the derivative signals (see Fig. 5) of each of the three ESR lines of D atoms

on the square root of the microwave power entering the cavity. Each of the experimental lines for D atoms in Im-He samples was fitted by a Lorentzian curve. From these fits the amplitudes and linewidths were obtained. Only for the smallest powers ( $\leq 0.25 \mu\text{W}$ ) is  $\Delta H_{pp}$  constant and the amplitude  $A_{pp} \propto \sqrt{P_c}$  as expected for an unsaturated ESR transition. For microwave power  $P_c \geq 0.25 \mu\text{W}$  the linewidths of all lines grow, although in the D-D<sub>2</sub>-Ne-He sample the degree of saturation of the side lines is larger than for the central line [see Fig. 6(a)]. Investigation of the behavior of linewidths and peak-to-peak amplitudes of the D atom ESR derivative signals as functions of the square root of the microwave power allows us to estimate the times for spin-spin relaxation ( $T_2$ ) and spin-lattice relaxation ( $T_1$ ) of D atoms in Im-He solids. The spin-spin relaxation time is calculated from the linewidth below saturation by means of the expression<sup>34</sup>

$$T_2 = \frac{1.3131 \times 10^{-7}}{g \Delta H_{pp}}, \quad (12)$$

where  $g$  is the electronic  $g$  factor and  $\Delta H_{pp}$  is the linewidth obtained from the peak-to-peak separation for the derivative ESR signal. For the D-D<sub>2</sub>-He sample, the linewidth at the lowest power is 1.5 G [see Fig. 6(a)], giving a value of  $T_2 = 4.4 \times 10^{-8}$  s. For estimating the value of  $T_1$  we determined the maximum value of the peak amplitude of the derivative signal in the Fig. 6(b). The value of  $T_1$  was then calculated by means of the expression<sup>34</sup>

$$T_1 = \frac{1.97 \times 10^{-7} \Delta H_{pp}}{g H_1^2}, \quad (13)$$

where  $H_1$  is the magnitude of the microwave magnetic field in the cavity when the amplitude of the ESR signal is a maximum. From Fig. 6(b) the value of the power corresponding to the maximum amplitude of the signal is  $P_{cm} = 6.25 \mu\text{W}$ . The relation between the microwave magnetic field and the microwave power absorbed in the cavity  $P_c$  is<sup>34</sup>

$$H_1^2 = 2 \times 10^{-3} P_c Q \eta \frac{V_c}{V_s}, \quad (14)$$

where  $H_1$  is the microwave field in gauss,  $P_c$  is the microwave power in watts,  $Q$  is the cavity quality factor,  $\eta$  is the filling factor,  $V_c = 8.3 \text{ cm}^3$  is the cavity volume, and  $V_s = 0.35 \text{ cm}^3$  is the sample volume. The filling factor  $\eta = 0.062$  for our sample in the quartz lined cavity with  $Q = 2700$  was calculated by using a computer program CST MICROWAVE STUDIO™. When we placed the above parameters into Eq. (14) it became

$$H_1^2 = 7.9 P_c. \quad (15)$$

From Eqs. (13) and (15) for D atoms in the D-D<sub>2</sub>-He sample for  $P_c = 6.25 \mu\text{W}$ , we estimate  $T_1 = 3 \times 10^{-3}$  s. Similar analysis of the results for D atoms in the D-D<sub>2</sub>-Ne-He sample gave lower values for  $T_2 = 3.1 \times 10^{-8}$  s and  $T_1 = 0.727 \times 10^{-3}$  s. The relatively small values of  $T_1$  for D atoms in Im-He solids confirm that the atoms are captured in clusters of D<sub>2</sub> molecules rather than isolated in liquid and

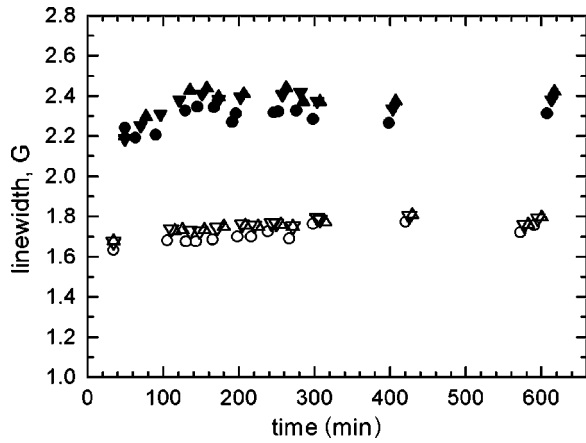


FIG. 7. Time dependence of the linewidths of hyperfine components for D atoms in D-D<sub>2</sub>-He solid (sample No. 2, Table I) ( $\nabla$ :  $I_z = +1$ ,  $\circ$ :  $I_z = 0$ ,  $\triangle$ :  $I_z = -1$ ) and in D-D<sub>2</sub>-Ne-He solid (sample No. 4, Table I) (closed  $\nabla$ :  $I_z = +1$ , closed  $\circ$ :  $I_z = 0$ , closed  $\triangle$ :  $I_z = -1$ ) obtained at temperature  $T = 1.375$  K and microwave power  $P_c = 2.25$   $\mu$ W.

solid helium. In the latter case the  $T_1$  value would be much larger. For example isolated Cs atoms in solid helium have  $T_1 \sim 1-2$  s.<sup>39</sup>

We observed saturation of ESR signals of D atoms in Im-He solids at lower microwave power levels ( $P_c \sim 6.25$   $\mu$ W) than were needed to saturate D atoms in a solid D<sub>2</sub> matrix ( $P_c \sim 1000$   $\mu$ W)<sup>38</sup> at the same temperature ( $T \sim 1.35$  K). This observation might be explained by the disorder in the D<sub>2</sub> within the nanoclusters in Im-He solids disrupting spin-lattice relaxation between magnetic sublevels of D atoms. Other explanations, such as changes in the phonon spectrum due to the small cluster size, and deuterium atoms residing on the surface of the clusters, are also possible.

### 3. Shape and widths of ESR lines of D atoms in Im-He solids

The ESR absorption lines of D atoms stabilized in D-D<sub>2</sub>-He and D-D<sub>2</sub>-Ne-He solids are fitted well by Lorentzian curves, giving parameters of amplitude and width. The time dependence of the linewidths of D atoms in different Im-He solids during evolution of the samples is shown in Fig. 7. A small increase over time of the linewidth of D atoms in the D-D<sub>2</sub>-Ne-He sample was observed at  $T = 1.375$  K. After two hours the linewidths of the D atoms became equal to 2.2–2.4 G in the D-D<sub>2</sub>-Ne-He sample and 1.7–1.8 G in the D-D<sub>2</sub>-He sample. The broadening of the ESR lines of trapped free radicals in a solid matrix is determined by spin-lattice relaxation, spin density, matrix anisotropy, interaction with nuclei of neighboring molecules, and the experimental conditions under which the data were taken (degree of saturation, rate of passage, and the modulation parameters). In our experiments we used conditions which did not broaden the natural linewidth of D atoms in Im-He solids, so we could attempt to determine the dipole-dipole broadening due to the electron spin-spin interactions between D atoms. In one experiment, while warming a D-D<sub>2</sub>-He sample with initial D atom concentration  $4.5 \times 10^{17}$  per cm<sup>3</sup> from 1.35 K to 4 K we observed a decrease of the average concentration of the D at-

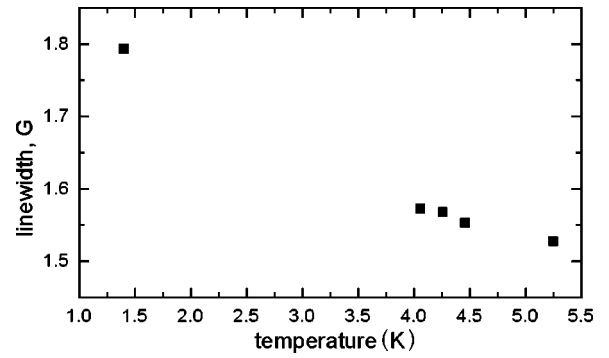


FIG. 8. Temperature dependence of the width of ESR lines of D atoms in a D-D<sub>2</sub>-He solid (sample No. 3, Table I).

oms down to  $2 \times 10^{16}$  cm<sup>-3</sup> and the width of ESR lines from 1.8 to 1.55 G (see Fig. 8). We can estimate the local concentration of D atoms in D<sub>2</sub> clusters by assuming that the decrease of the line width is due to the reduction of the dipole-dipole interaction between the D atoms. The dipole-dipole broadening of ESR lines in an fcc lattice is given by<sup>40</sup>

$$\Delta H_{dd} = 2.3g\mu_0\sqrt{S(S+1)}n_l, \quad (16)$$

where  $\Delta H_{dd}$  is in gauss and  $n_l$  is the concentration of atoms of spin  $S$ . Hence for D atoms in an fcc lattice  $n_l = 2.7 \times 10^{19} \Delta H_{dd}$ . From the results shown in Fig. 8 the value of  $\Delta H_{dd}$  is found to be equal to 0.25 G, so the local concentration of D atoms in a cluster is found to be at least  $n_l = 6.7 \times 10^{18}$  cm<sup>-3</sup>.

### 4. Measurements of D atom concentrations

By doubly integrating the derivatives of the ESR absorption lines of D atoms and ruby reference signals, we estimated the average concentration of D atoms in impurity-helium samples. The time dependences of the average concentrations of D atoms in our D-D<sub>2</sub>-He samples and D-D<sub>2</sub>-Ne-He sample are displayed in Fig. 9. Usually concen-

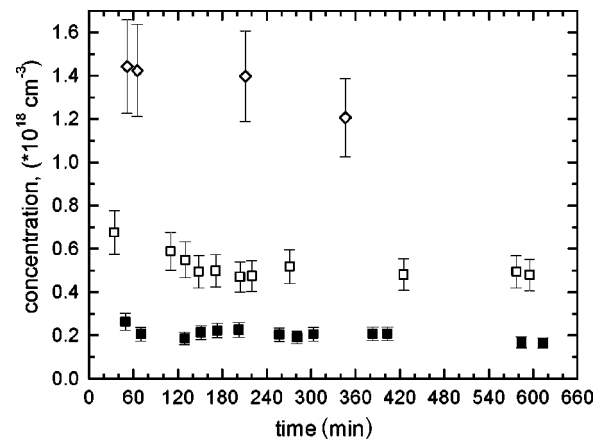


FIG. 9. Time dependence of the average concentration of D atoms (at  $T = 1.375$  K) in Im-He samples prepared from gas mixtures  $[D_2]:[He] = 1:20$  (open diamonds, sample No. 1, Table I),  $[D_2]:[He] = 1:100$  (open squares, sample No. 2, Table I) and  $[D_2]:[Ne]:[He] = 4:1:500$  (closed squares, sample No. 4, Table I).

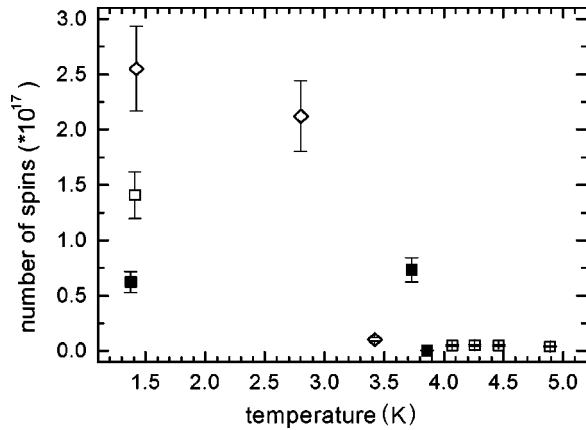


FIG. 10. The temperature dependence of the number of D atoms in different Im-He solids: sample No. 1 (open diamonds) and sample No. 2 (open squares) are D-D<sub>2</sub>-He solids, sample No. 4 (closed squares) is a D-D<sub>2</sub>-Ne-He solid.

trations of D atoms in D-D<sub>2</sub>-He samples were larger than in D-D<sub>2</sub>-Ne-He samples. The highest average concentration of D atoms stabilized in D-D<sub>2</sub>-He solids shortly after preparation,  $1.5 \times 10^{18} \text{ cm}^{-3}$ , was achieved in experiments on samples created from the gas mixture  $[\text{D}_2]:[\text{He}]=1:20$ . The impurity-helium solids with these high concentrations of D atoms were very stable in superfluid helium at  $T=1.375 \text{ K}$  during the full time of observation ( $\sim 300 \text{ min}$ ).

Figure 10 shows the results of measuring the numbers of D atoms in dry Im-He samples at different temperatures. Usually the first measurement of the number of atoms in dry samples at  $T \sim 2\text{--}2.5 \text{ K}$  gave results similar to those for the wet sample. Further increasing the temperature of the samples initiated diffusion of D atoms and their recombination. For example, in one dry D-D<sub>2</sub>-He sample formed from gas mixture  $[\text{D}_2]:[\text{He}]=1:20$  a small decrease in the number of D atoms was observed at  $T=2.8 \text{ K}$ . The complete destruction of this dry D-D<sub>2</sub>-He sample occurred at  $T \sim 3.4 \text{ K}$ . At this temperature the number of D atoms decreased more than one order of magnitude from  $2.1 \times 10^{17}$  to  $2.0 \times 10^{16}$ . Microcrystallites of solid deuterium form from merging D<sub>2</sub> nanoclusters as the D<sub>2</sub>-He sample collapses.<sup>10</sup> Only very low concentrations of stabilized D atoms survived within these microcrystallites. The number of D atoms stabilized in these microcrystallites was constant in the temperature range  $T \sim 4.0\text{--}5.3 \text{ K}$ . The process of destruction of Im-He solids is rather fast. By using the CW ESR method we are only able to precisely register the signals of stabilized atoms just before and just after destruction of the Im-He solids. To investigate the fast process of destruction of the Im-He solids we are planning to use a pulsed x-band ESR apparatus, the construction of which is now under way in our laboratory.

#### IV. DISCUSSION

The results obtained by x-ray scattering for D<sub>2</sub>-He and D<sub>2</sub>-Ne-He solids and by ESR spectroscopy for D-D<sub>2</sub>-He and D-D<sub>2</sub>-Ne-He solids allow us to reach important conclusions

about the structure of these solids. X-ray-diffraction measurements show that our samples are built of D<sub>2</sub> and Ne blocks with a nanometer-scale characteristic size. The best agreement with the experimental x-ray data for the dry D<sub>2</sub>-He solids shown in Fig. 2 was obtained for a collection of  $\sim 90 \text{ \AA}$  clusters each consisting of  $\sim 11\,500$  D<sub>2</sub> molecules arranged in randomly stacked and fault containing fcc structures. The average density of D<sub>2</sub> in the dry D<sub>2</sub>-He sample is found to be  $2.5 \times 10^{21} \text{ molecules/cm}^3$ . For the as-prepared D<sub>2</sub>-He samples the intensity of the D<sub>2</sub> cluster peak is very small (approximately 1/10 that of the dry sample). It is difficult to determine the size of the clusters in this case because of poor signal to noise ratio. Assuming that the cluster sizes in the as-prepared sample are equal to those in the dry sample, we find that the average density of D<sub>2</sub> molecules in the as-prepared sample is  $\sim 10^{20} \text{ cm}^{-3}$ . However, due to the weak diffraction signal, deuterium clusters significantly smaller than  $90 \text{ \AA}$  cannot be experimentally detected in the as-prepared D<sub>2</sub> samples. Thus, the actual D<sub>2</sub> density in this sample can be significantly larger than  $10^{20} \text{ cm}^{-3}$ .

Analysis of x-ray data for the as-prepared mixed D<sub>2</sub>-Ne-He sample (see Fig. 4) shows that separate nanoclusters of D<sub>2</sub> molecules and Ne atoms are present in the sample. The experimental diffraction pattern is best described by a superposition of peaks originating from  $\sim 50 \text{ \AA}$  Ne fcc clusters and  $\sim 75 \text{ \AA}$  D<sub>2</sub> fcc clusters. In both cases the clusters were found to contain stacking faults. The densities of molecular deuterium and atomic neon were found to be  $7 \times 10^{20} \text{ molecules/cm}^3$  and  $3 \times 10^{19} \text{ atoms/cm}^3$ , respectively. In the mixed D<sub>2</sub>-Ne-He solids, the clusters appear to contain a larger fraction of D<sub>2</sub> as compared with Ne ( $[\text{D}_2]/[\text{Ne}]=23$ ) than was present in the gas jet used for the sample preparation ( $[\text{D}_2]/[\text{Ne}]=4$ ). This fact may be explained by the presence of very small Ne clusters in these samples, which would have given a very broad x-ray-diffraction signal but would not have substantially contributed to the main peak of Ne clusters. We have no other evidence for this, however, and we believe that further experiments are required to resolve this discrepancy.

X-ray scattering studies show that the D<sub>2</sub>-He and D<sub>2</sub>-Ne-He samples are highly porous solids with typical building blocks in the nanometer size range. During draining of the liquid helium from the samples, we observed growth in the size of the D<sub>2</sub> clusters and an increase of the average density of D<sub>2</sub> molecules in the sample. The highest density is found to be  $2.5 \times 10^{21} \text{ molecules/cm}^3$  in the dry D<sub>2</sub>-He sample. A significant amount of helium is found to be trapped in the dry D<sub>2</sub>-He sample at low temperatures ( $1.5\text{--}3.2 \text{ K}$ ), and a large fraction of this helium is adsorbed on the sample internal surfaces. The adsorbed helium may be an important factor preventing the coalescence of D<sub>2</sub> clusters and collapse of our highly porous samples.

The highly porous D<sub>2</sub>-He solids are very promising for the production of high concentrations of ultracold neutrons at very low temperatures. As proposed in Ref. 23, the cold neutrons are effectively cooled by collisions with nanoclusters of low-absorbing materials at  $T=1 \text{ mK}$ . Major cryogenic problems must be solved for this technique to be viable.

Another possible application of porous D<sub>2</sub>-He solids is the achievement of significant nuclear polarization of the D<sub>2</sub> molecules at low temperatures by the brute-force method.<sup>24–26</sup> The latter may be important to applications of nuclear fusion because of the increase by 50% of the cross section of the neutron-lean reaction for nuclear-spin polarized reagents.<sup>41</sup> The small clusters provide a very large surface area, leading to intimate thermal contact between the D<sub>2</sub> molecules and an external helium bath. The lowest energy rotational state of D<sub>2</sub> will be  $J=0$ . This state will contain  $I=0$  and  $I=2$  nuclear spin states in the proportion 1:5. The  $I=2$  molecules will be spin active down to the lowest temperatures so that substantial nuclear polarizations can be achieved in magnetic fields of 10 T at temperatures near 3 mK, which can be reached with a well designed dilution refrigerator.

An important motivation for studies of atomic deuterium in impurity-helium solids has been the possibility of achieving high local concentrations of atomic deuterium. High concentrations of D atoms in D-D<sub>2</sub> nanoclusters might give rise to quantum overlap of the deuterium atom wave functions. To work toward this goal, we carried out investigations of D atoms stabilized in D-D<sub>2</sub>-He and D-D<sub>2</sub>-Ne-He solids by ESR. It was found that the  $g$  factors and hyperfine interactions of D atoms in the D-D<sub>2</sub>-He solids and in the D-D<sub>2</sub>-Ne-He solids are similar to each other and very close to those obtained for D atoms stabilized in a solid D<sub>2</sub> matrix.<sup>32,37</sup> From the investigation of the saturation behavior of the ESR lines of the D atoms, a relatively short spin-lattice relaxation time,  $T_1=3\times 10^{-3}$  s, was found. All these observations show that D atoms were mainly stabilized inside D<sub>2</sub> clusters. This result is further corroborated by ESR studies of Im-He solids containing H and D atoms along with H<sub>2</sub> and D<sub>2</sub> molecules. Satellite ESR lines on H and D resonances were associated with simultaneous spin flips of atomic electrons and protons on neighboring HD and H<sub>2</sub> molecules.<sup>16</sup> We have measured the average concentrations of D atoms via ESR in D-D<sub>2</sub>-He and D-D<sub>2</sub>-Ne-He samples. For as-prepared D-D<sub>2</sub>-He samples the highest average concentration of D atoms achieved was  $1.5\times 10^{18}$  cm<sup>-3</sup>. The draining of the liquid helium from the D-D<sub>2</sub>-He sample at  $T=1.5\text{--}2.5$  K does not usually change the concentration of the stabilized D atoms. Using the D<sub>2</sub> density in the dry samples obtained in the x-ray measurements ( $2.5\times 10^{21}$  cm<sup>-3</sup>), and assuming that all the stabilized D atoms reside in the D<sub>2</sub> clusters, we estimate that the relative concentration of D atoms in D<sub>2</sub> clusters is

$$n_D = \frac{[D]}{[D_2]} = \frac{1.5\times 10^{18} \text{ cm}^{-3}}{2.5\times 10^{21} \text{ cm}^{-3}} = 6\times 10^{-4}. \quad (17)$$

The density of deuterium molecules within the clusters should be similar to the density of bulk solid deuterium. Therefore the local concentration of D atoms in D<sub>2</sub> clusters can be determined as

$$n_l = N n_D = (3\times 10^{22} \text{ cm}^{-3})(6\times 10^{-4}) = 1.8\times 10^{19} \text{ cm}^{-3} \quad (18)$$

( $N$  is the number of D<sub>2</sub> molecules in 1 cm<sup>3</sup> of solid deuterium). There are approximately seven stabilized D atoms in a typical D<sub>2</sub> cluster, which has a diameter of 90 Å ( $N\sim 11\,500$  molecules of D<sub>2</sub>).

As discussed above, our x-ray experiments on the as-prepared D<sub>2</sub> samples provide only a rough estimate of the lowest possible D<sub>2</sub> concentration. Using this estimate ( $\sim 10^{20}$  cm<sup>-3</sup>), we find that the relative concentration of the D atoms in the D<sub>2</sub> clusters should be

$$n_D = \frac{[D]}{[D_2]} = \frac{1.5\times 10^{18} \text{ cm}^{-3}}{10^{20} \text{ cm}^{-3}} = 1.5\times 10^{-2}. \quad (19)$$

Using Eq. (18), we find that the local concentration of the D atoms calculated in this approximation is very large:  $n_l\sim 4.5\times 10^{20}$  cm<sup>-3</sup>. Such a large value of  $n_l$  clearly contradicts the result  $n_l=0.67\times 10^{19}$  cm<sup>-3</sup> obtained from the decreasing ESR linewidth of D atoms during the destruction of our D-D<sub>2</sub>-He sample. These observations are consistent with our previous remark that x-ray measurements may grossly underestimate the density of the as-prepared D<sub>2</sub> samples if one assumes that the D<sub>2</sub> cluster size is the same as that in the dry samples. These results, therefore, provide possible evidence that most of the D<sub>2</sub> clusters in the as-prepared D<sub>2</sub> samples are smaller than 90 Å.

In the mixed D<sub>2</sub>-Ne-He sample immersed in liquid helium, the density of D<sub>2</sub> molecules is  $7.5\times 10^{20}$  cm<sup>-3</sup> as obtained from the x-ray results. If we again assume that all D atoms are stabilized in D<sub>2</sub> clusters, then the relative concentration of the D atoms is  $n_D=2\times 10^{17}/7.5\times 10^{20}=2.6\times 10^{-4}$ . The local concentration of D atoms may be calculated as  $n_l=(3\times 10^{22})(2.6\times 10^{-4})=8\times 10^{18}$  cm<sup>-3</sup>. For comparison, the local concentration calculated from the ESR linewidth of D atoms is  $6.7\times 10^{18}$  cm<sup>-3</sup>. These two values are in agreement with each other, confirming the accuracy of the determination of the D<sub>2</sub> density by the x-ray method when the diffraction signals are large enough. In these samples, the number of D atoms in each D<sub>2</sub> cluster ( $N\sim 9000$  molecules of D<sub>2</sub>) is equal to two. Hence this system should be very stable at low temperatures. The very small number of deuterium atoms in a cluster is taken to be a consequence of the very small size of the D-D<sub>2</sub> nanoclusters. All Im-He solids investigated which contained stabilized D atoms were stable in superfluid helium. Even after draining liquid helium from these porous samples at  $T\sim 2\text{--}3.2$  K the Im-He solids still maintained stable concentrations of D atoms. Only after warming the dry samples above 3.4 K did complete destruction of the samples occur, with rapid recombination of most of the stabilized D atoms.

If the atoms in the clusters were free and sufficiently numerous, then effects associated with quantum overlap could be observed. For a dry D-D<sub>2</sub>-He sample with a local concentration of D atoms  $n_l=1.8\times 10^{19}$  atoms/cm<sup>3</sup> the mean distance between atoms inside D<sub>2</sub> clusters is  $d_m=10^8/\sqrt[3]{n_l}$  Å  $\sim 38$  Å. The thermal de Broglie wavelength,

$$\Lambda(T) = \sqrt{\frac{2\pi\hbar^2}{mkT}}, \quad (20)$$

for free D atoms then will be comparable to the mean distance between atoms at  $T=175$  mK.

Larger nanoclusters containing high *local* concentrations of D atoms are probably needed to supply a sufficient number of atoms to manifest effects of quantum overlap. Alternatively, one could work at very low temperatures where the *average* concentration of D atoms throughout the sample could provide enough quantum overlap. Unfortunately, D atoms have a very slow recombination rate in Im-He solids as demonstrated in our ESR experiments. This indicates that the D atoms are highly localized within the clusters and also have little likelihood of jumping from cluster to cluster. Therefore we are pessimistic about the possibility of observing effects of quantum overlap and the potential for seeing any manifestation of Fermi-Dirac statistics. On the other hand, studies of the D-D<sub>2</sub>-He impurity-helium solids can provide some guidance in preparing for investigations of the H-H<sub>2</sub>-He impurity-helium solids, which are more likely to manifest quantum overlap effects.

The difference in behavior of atomic hydrogen impurities compared with atomic deuterium impurities are quite significant. In the Im-He solids containing Ne and H atoms, the recombination of hydrogen was found to be quite rapid, in spite of the fact that the hydrogen was extremely dilute. On the other hand, very slow recombination rates for D atoms were observed in previous work<sup>16</sup> and this work (see Fig. 9). The discrepancy between the speeds of H atom recombination and D recombination deserves further investigation. This may be related to the extreme difference in the exchange tunneling reaction rates for  $D+D_2 \rightarrow D_2+D$  and  $H+H_2 \rightarrow H_2+H$  as calculated by Takayanagi *et al.*,<sup>42</sup> who calculated that the hydrogen reaction proceeds four orders of magnitude faster than that for deuterium. The difference implies that the H atoms in H<sub>2</sub> clusters are far more delocalized<sup>21</sup> than D atoms in D<sub>2</sub> clusters. On the basis of this delocalization the hydrogen atoms are much more likely to interact and overlap with each other, leading to possible quantum fluid behavior. Another question that must be considered is whether or not hydrogen atoms can travel between H<sub>2</sub> clusters.

Thus the Im-He solids provide us with two different model quantum systems. The first, a boson system, corresponds to the Im-He solids containing delocalized hydrogen atoms. The second, a fermion system, corresponds to the Im-He solids containing much higher concentrations of heavier and more localized deuterium atoms. The best that can be hoped for is that H atoms in Im-He solids can undergo

Bose-Einstein condensation. This is very speculative. Unfortunately it is less likely that quantum fluid behavior can be exhibited in Im-He solids containing D atoms.

## V. CONCLUSIONS

The light impurity-helium solids created by introducing deuterium atoms and molecules into superfluid helium have been investigated by x-ray diffraction and ESR methods. D atoms are mainly stabilized in D<sub>2</sub> clusters with sizes  $\sim 75\text{--}90$  Å. The average density of D<sub>2</sub> molecules in impurity-helium solids is  $\sim 10^{21}$  cm<sup>-3</sup>. These small clusters of deuterium assemble into a porous gel-like structure in a manner similar to the case for the impurity-helium solids containing heavier atoms and molecules. In this quantum system, clusters with high local concentrations of stabilized D atoms can be created. In the clusters with the highest local concentration ( $\sim 1.8 \times 10^{19}$  cm<sup>-3</sup>) observed in this work, the mean distance between D atoms inside D<sub>2</sub> clusters is  $\sim 38$  Å. From the long recombination times we find in this work, the D atoms seem to be rather well localized so that their quantum overlap effects may be severely limited in Im-He solids, as opposed to the case for free D atoms. A somewhat more promising situation seems to exist for H atoms, which at least in the case of a H-H<sub>2</sub>-Ne impurity-helium solid, have a much more rapid recombination rate, indicating possible delocalization. Im-He solids with only H and H<sub>2</sub> impurities are difficult to achieve, but this will be the subject of future research in this laboratory.

Impurity-helium solids containing D<sub>2</sub> molecules may be used to achieve high deuterium nuclear polarizations. In this work, we have demonstrated that the D<sub>2</sub> molecules tend to cluster in tiny crystallites  $\sim 90$  Å, which gives large net surface areas, thereby providing extremely efficient heat transport. This allows for cooling the sample to very low temperatures in high magnetic fields (brute force polarization). Finally, impurity-helium solids containing D<sub>2</sub> may be eventually used to enhance a flux of ultracold neutrons.

## ACKNOWLEDGMENTS

We would like to thank NASA for its support through Grant No. NAG 3-2871. This work was also supported by North Atlantic Treaty Organization under a grant awarded in 2002 (R.E.B.), and by the A. P. Sloan Foundation (V.K.). We also wish to thank P. Borbat and G. Codner for extremely useful conversations and help with the ESR experiments, and B. Keimer for the use of his x-ray cryostat.

<sup>1</sup>E.B. Gordon, V.V. Khmelenko, A.A. Pelmenov, E.A. Popov, and O.F. Pugachev, *Chem. Phys. Lett.* **155**, 301 (1989).

<sup>2</sup>E.B. Gordon, V.V. Khmelenko, A.A. Pelmenov, E.A. Popov, O.F. Pugachev, and A.F. Shestakov, *Chem. Phys.* **170**, 411 (1993).

<sup>3</sup>J.D. Reppy, *J. Low Temp. Phys.* **87**, 205 (1992).

<sup>4</sup>J. Yoon, D. Sergatskov, J. Ma, N. Mulders, and M.H.W. Chan, *Phys. Rev. Lett.* **80**, 1461 (1998).

<sup>5</sup>E.B. Gordon, A.A. Pelmenov, O.F. Pugachev, V.L. Tal'roze, and

V.V. Khmelenko, *Dokl. Phys. Chem.* **280**, 145 (1985).

<sup>6</sup>E.B. Gordon, A.A. Pelmenov, O.F. Pugachev, and V.V. Khmelenko, *JETP Lett.* **37**, 282 (1983).

<sup>7</sup>E.B. Gordon, A.A. Pelmenov, O.F. Pugachev, and V.V. Khmelenko, *Sov. J. Low Temp. Phys.* **11**, 307 (1985).

<sup>8</sup>V. Kiryukhin, B. Keimer, R.E. Boltnev, V.V. Khmelenko, and E.B. Gordon, *Phys. Rev. Lett.* **79**, 1774 (1997).

<sup>9</sup>S.I. Kiselev, V.V. Khmelenko, D.M. Lee, V. Kiryukhin, R.E. Bolt-

- nev, E.B. Gordon, and B. Keimer, *J. Low Temp. Phys.* **126**, 235 (2002).
- <sup>10</sup>S.I. Kiselev, V.V. Khmelenko, D.M. Lee, V. Kiryukhin, R.E. Boltnev, E.B. Gordon, and B. Keimer, *Phys. Rev. B* **65**, 024517 (2002).
- <sup>11</sup>S.I. Kiselev, V.V. Khmelenko, D.A. Geller, J.R. Beamish, and D.M. Lee, *Physica B* **284-288**, 105 (2000).
- <sup>12</sup>S.I. Kiselev, V.V. Khmelenko, D.A. Geller, D.M. Lee, and J.R. Beamish, *J. Low Temp. Phys.* **119**, 357 (2000).
- <sup>13</sup>S.I. Kiselev, V.V. Khmelenko, and D.M. Lee, *Low Temp. Phys.* **26**, 641 (2000).
- <sup>14</sup>S.I. Kiselev, V.V. Khmelenko, and D.M. Lee, *J. Low Temp. Phys.* **121**, 671 (2000).
- <sup>15</sup>S.I. Kiselev, V.V. Khmelenko, D.M. Lee, and C.Y. Lee, *J. Low Temp. Phys.* **128**, 37 (2002).
- <sup>16</sup>S.I. Kiselev, V.V. Khmelenko, and D.M. Lee, *Phys. Rev. Lett.* **89**, 175301 (2002).
- <sup>17</sup>V.V. Khmelenko, S.I. Kiselev, D.M. Lee, and C.Y. Lee, *Phys. Scr. T* **102**, 118 (2002).
- <sup>18</sup>S.I. Kiselev, V.V. Khmelenko, E.P. Bernard, C.Y. Lee, and D.M. Lee, *Physica B* **329-333**, 377 (2003).
- <sup>19</sup>S.I. Kiselev, V.V. Khmelenko, E.P. Bernard, and D.M. Lee, *Low Temp. Phys.* **29**, 678 (2003).
- <sup>20</sup>S.I. Kiselev, V.V. Khmelenko, C.Y. Lee, and D.M. Lee, *J. Low Temp. Phys.* **121**, 677 (2000).
- <sup>21</sup>T. Miyazaki, K.-P. Lee, K. Fueki, and A. Takeuchi, *J. Phys. Chem.* **88**, 4959 (1984).
- <sup>22</sup>E.P. Bernard, R.E. Boltnev, V.V. Khmelenko, and D.M. Lee, *J. Low Temp. Phys.* **134**, 175 (2004).
- <sup>23</sup>V.V. Nesvizhevsky, *Phys. At. Nucl.* **65**, 400 (2002).
- <sup>24</sup>E. ter Haar, G. Frossati, and W.G. Clark, *J. Low Temp. Phys.* **94**, 361 (1994).
- <sup>25</sup>G. Frossati, *J. Low Temp. Phys.* **111**, 521 (1998).
- <sup>26</sup>R.E. Boltnev, G. Frossati, E.B. Gordon, I.N. Krushinskaya, E.A. Popov, and A. Usenko, *J. Low Temp. Phys.* **27**, 245 (2002).
- <sup>27</sup>J.L. Yarnell, R.L. Mills, and A.F. Schuch, *Sov. J. Low Temp. Phys.* **1**, 366 (1975).
- <sup>28</sup>B.E. Warren, *X-ray Diffraction* (Addison-Wesley, Reading, MA, 1969).
- <sup>29</sup>I.F. Silvera, *Rev. Mod. Phys.* **52**, 393 (1980).
- <sup>30</sup>E. Cheng, G. Ihm, and M.W. Cole, *J. Low Temp. Phys.* **74**, 519 (1989).
- <sup>31</sup>G. Breit and I.I. Rabi, *Phys. Rev.* **38**, 2082 (1931).
- <sup>32</sup>M. Sharnoff and R.V. Pound, *Phys. Rev.* **132**, 1003 (1963).
- <sup>33</sup>P.J. Mohr and B.N. Taylor, *Rev. Mod. Phys.* **72**, 351 (2000).
- <sup>34</sup>C.P. Poole, Jr., *Electron Spin Resonance. A Comprehensive Treatise on Experiment Techniques* (Interscience, New York, 1967).
- <sup>35</sup>A.G. Prodel and P. Kusch, *Phys. Rev.* **79**, 1009 (1950); **88**, 184 (1952).
- <sup>36</sup>C.K. Jen, S.N. Foner, E.L. Cochran, and V.A. Bowers, *Phys. Rev.* **112**, 1169 (1958).
- <sup>37</sup>L.B. Knight Jr., W.E. Rice, L. Moore, E.R. Davidson, and R.S. Dailey, *J. Chem. Phys.* **109**, 1409 (1998).
- <sup>38</sup>A.S. Iskovskikh, A.Ya. Katunin, I.I. Lukashevich, V.V. Sklyarevskii, V.V. Suraev, V.V. Filippov, N.I. Filippov, and V.A. Shevtsov, *Sov. Phys. JETP* **64**, 1085 (1986).
- <sup>39</sup>M. Arndt, S.I. Kanorsky, A. Weis, and T.W. Hansch, *Phys. Rev. Lett.* **74**, 1359 (1995).
- <sup>40</sup>C. Kittel and E. Abrahams, *Phys. Rev.* **90**, 238 (1953).
- <sup>41</sup>M.P. Rekaló and E. Tomasi-Gustafsson, *Phys. Rev. C* **57**, 2870 (1998).
- <sup>42</sup>T. Takayanagi, K. Nakamura, and S. Sato, *J. Chem. Phys.* **90**, 1641 (1989).